RESEARCH ARTICLE
doi: 10.2306/scienceasia1513-1874.2025.093

*ScienceAsia* 51 (6): 2025: ID 2025093: **1–9**

# Determination of intrinsic second-order rate constant for acetophenone in reaction with hydroxyl radicals and its temperature-correction coefficients

**Napadsorn Rungruangsirinon, Jin Anotai, Nonglak Boonrattanakij***

Department of Environmental Engineering, Faculty of Engineering, King Mongkut's University of Technology Thonburi, Bangkok 10140 Thailand

*Corresponding author, e-mail: nonglak.boo@kmutt.ac.th

*Received 18 Apr 2025, Accepted 6 Nov 2025*
*Available online 22 Dec 2025*

**ABSTRACT**: Acetophenone is a refractory organic pollutant found in several industrial wastewaters. It can escape biological secondary treatment systems and cause adverse impacts on aquatic ecology. Further treatment through advanced oxidation processes, which generate powerful hydroxyl radicals, is a promising option. The intrinsic second-order rate constant between acetophenone and hydroxyl radicals, as well as its temperature-correction coefficients, was determined using a homogeneous Fenton-like process at pH 2.5. Using the competitive kinetics technique with aniline as a reference compound, the intrinsic second-order rate constant for the reaction between acetophenone and hydroxyl radicals was determined to be $8.97\times10^9$ $M^{-1}s^{-1}$ at 25 °C and 1 atm. This value remained consistent across various scenarios involving different reactant concentrations, hydraulic retention times, and operating modes. Hydroxyl radicals can reach a quasi-steady state during the initial stage of the batch operation. Using the quasi-steady-state approximation and the initial rate technique, the previously unreported activation energy for the Arrhenius equation and the thermal coefficient for the Phelps empirical equation were determined to be 29 kJ/mol and 1.035, respectively, over the temperature range of 20–40 °C. The concentrations of hydroxyl radicals at the quasi-steady state of the batch reactor and at the steady state of the continuous-stirred tank reactor were found to range from $5.0\times10^{-14}$ and $1.1\times10^{-13}$ M. This information is very beneficial for reactor design and operational monitoring of acetophenone removal by advanced oxidation processes.

**KEYWORDS**: activation energy, Fenton-like, thermal coefficient

## INTRODUCTION

Acetophenone (AP) is an important industrial chemical utilized in various sectors, including the production of phenols, pharmaceuticals, perfumes, pesticides, and dyes [1]. It is characterized by its light-yellow liquid appearance, strong odor, and slight solubility in water under standard conditions. However, AP is also known to be toxic to aquatic life and can persist in aquatic environments for extended periods, posing a significant challenge to biological treatment methods [2]. Consequently, the development and adoption of advanced non-biological techniques for its removal from wastewater are imperative to mitigate its harmful effects on ecosystems.

Advanced oxidation processes (AOPs) have emerged as promising solutions for treating refractory organic pollutants like AP. AOPs are advantageous because they produce hydroxyl radicals (OH•), which are highly reactive and non-selective oxidants with a high oxidation potential [3, 4]. Through these processes, complex organic structures can be oxidized, leading to their transformation into simpler biodegradable molecules or complete mineralization into carbon dioxide [5, 6]. To effectively simulate and monitor AP degradation by OH•, knowledge of its intrinsic rate constant is essential. The reaction kinetics between any pollutant and OH• can be described in a second-order manner [7], where both reactants follow first-order kinetics. The intrinsic second-order rate constant ($k$), typically reported at standard-state conditions (25 °C and 1 atm), holds universal applicability irrespective of varying reactant concentrations and system conditions [8]. This makes the intrinsic rate constant more practical than pseudo-zero- or first-order apparent rate constants, which are limited to specific experimental conditions.

While several studies have documented the rapid oxidation of AP by OH• in aqueous phases using various AOP technologies, e.g., ordinary Fenton process [9], indirect ozonation [10, 11], and photocatalysis [12, 13], there has been a lack of comprehensive data on the intrinsic second-order rate constant ($k_{AP,\,OH\bullet}$). The only noted result comes from Boonrattanakij et al [9], who performed measurements using the ordinary Fenton process at pH 3.0. This study aimed to verify and expand upon these findings by determining the intrinsic rate constant under a homogeneous Fenton-like process at pH 2.5. The research also explored the influence of temperature (20 to 40 °C) on the rate constant and revealed previously undocumented temperature-correction coefficients derived from Arrhenius and Phelps empirical equations.

The traditional Fenton process facilitates the generation of OH• through the catalytic decomposition of hydrogen peroxide ($H_2O_2$) in the presence of ferrous

($Fe^{2+}$). This process consists of a series of complex reactions (Eqs. (1) to (6)) that systematically produce OH• as reactive oxidants for pollutant degradation [14].

$$Fe^{2+} + H_2O_2 \rightarrow Fe^{3+} + OH^{\bullet} + OH^{-} \quad (1)$$

$$Fe^{3+} + H_2O_2 \rightarrow Fe^{2+} + HO_2^{\bullet} + H^{+} \quad (2)$$

$$HO_2^{\bullet} \leftrightarrow O_2^{-\bullet} + H^{+} \quad (3)$$

$$Fe^{2+} + OH^{\bullet} \rightarrow Fe^{3+} + OH^{-} \quad (4)$$

$$H_2O_2 + OH^{\bullet} \rightarrow HO_2^{\bullet} + H_2O \quad (5)$$

$$RH + OH^{\bullet} \rightarrow R^{\bullet} + H_2O \rightarrow\rightarrow \text{products}/CO_2/H_2O \quad (6)$$

This research employed a homogeneous Fenton-like process that used ferric ions ($Fe^{3+}$) as the catalyst instead of $Fe^{2+}$. Despite the slower overall reaction rate of the Fenton-like process compared to the ordinary Fenton process, attributable to the necessity of converting $Fe^{3+}$ to $Fe^{2+}$ via reaction Eq. (2) prior to generating OH• in Eq. (1), the Fenton-like method is still deemed advantageous. Its widespread application stems from the enhanced stability and lower cost associated with using ferric salts compared to ferrous salts [15]. This favorable aspect has led to the adoption of the Fenton-like process in both secondary and tertiary treatment systems [16, 17] and its utility in sludge pretreatment [18]. The economic viability and ease of implementation further solidify its role in wastewater treatment practices.

To accurately measure the kinetics of AP degradation and mitigate potential interference from competitive reactions between OH• and oxidation intermediates arising from the transformation of AP, a competitive kinetics technique, validated in previous research [19], was employed. Aniline (AN) was used as a reference compound in this study due to not only its intrinsic rate constant with OH• ($k_{AN,\,OH^{\bullet}}$) is known ($4.8 \times 10^9$ 1/(M·s) [7]) but also it can be precisely quantified under similar methodologies and conditions as AP.

To further investigate the effect of temperature on the $k_{AP,\,OH^{\bullet}}$, the reaction conditions were varied within the range of 20 to 40 °C. This temperature variation is critical because it can influence both the reaction kinetics and the stability of intermediates formed during AP degradation. Initial rate technique was adopted to eliminate interference from these intermediates. The outcomes from these experiments will allow for a comprehensive understanding of how varying temperatures impact the reaction dynamics and the applicability of AOPs in real-world wastewater treatment scenarios. The findings will contribute significantly to optimizing the operational parameters needed for effective AP removal while reducing overall treatment costs and improving process efficiency.

## MATERIALS AND METHODS

### Chemicals and analytical methods

In this study, all chemicals utilized were of analytical grade, ensuring high purity for experimental reliability. The specific chemicals included: anhydrous ferric sulfate ($Fe_2(SO_4)_3$, Carlo Erba, Val de Reuil, France), ferrous sulfate heptahydrate ($FeSO_4 \cdot 7\,H_2O_2$, Carlo Erba), hydrogen peroxide ($H_2O_2$, 35% w/w, Sigma-Aldrich, Massachusetts, USA), acetophenone (AP, Sigma-Aldrich), and aniline (AN, Sigma-Aldrich). These chemicals were employed without any pretreatment. For pH adjustments before and during the experiments, sulfuric acid ($H_2SO_4$) and sodium hydroxide (NaOH) solutions prepared at various concentrations were used. All solutions and reagents were prepared using deionized water to avoid any potential contaminations.

Iron concentrations were analyzed using colorimetric methods as per the guidelines set forth by APHA [20]. Concentration of $H_2O_2$ was determined through iodometric titration based on the methodology outlined by Brandhuber and Korshin [21]. Concentrations of AP and AN were quantified using gas chromatography (GC2030, Shimadzu, Japan), equipped with a flame ionization detector and a capillary column (0.53 mm diameter × 30 m length × 1.50 µm film thickness, HP-5, Hewlett-Packard, USA). A sample volume of 1.0 µl was injected into the injection port. The column temperature was initially set to 110 °C for the first 1.5 min, then increased by 15 °C/min to 163 °C, followed by a more rapid increase of 40 °C/min until 270 °C, and maintained for an additional 5 min. Injector and detector temperatures were held at 250 °C and 270 °C, respectively.

### Experimental setup

To ensure the reliability and accuracy of the $k_{AP,\,OH^{\bullet}}$, this study employed both batch reactors and continuous stirred tank reactors (CSTR) with varied configurations. This dual approach allows for comprehensive validation of the experimental results, leveraging the strengths of each reactor type to obtain precise kinetic measurements.

In the batch study, a 600-ml Pyrex beaker equipped with a magnetic stirrer to facilitate effective mixing was utilized throughout the experiment. The process began with the addition of a well-defined solution containing the target concentrations of $Fe^{3+}$, AP, and AN into the reactor, which was measured to a total volume of 500 ml. To promote the complete dissolution of $Fe_2(SO_4)_3$, the pH of the solution was adjusted to 2.5 using $H_2SO_4$. Throughout the process, the pH was continuously monitored and adjusted as needed, either by $H_2SO_4$ or NaOH addition. Temperature was another key factor in this study; thus, it was maintained at precise levels of 20, 25, 30, 35, and 40 °C using a controlled water bath. The reaction was initiated by

the addition of a predetermined amount of $H_2O_2$ to trigger the desired chemical transformations.

To monitor the reaction kinetics effectively, several samples were taken at designated time intervals. Two samples were concurrently withdrawn using two micropipettes. The first sample was promptly injected into a sample tube containing 2 ml of 0.1 M NaOH, which served to precipitate iron ions and effectively terminated any further progress of the Fenton reaction. This step was crucial for preparing the sample for subsequent analysis of residual organic compounds. The second sample, on the other hand, was subjected to immediate analysis for the concentrations of iron and $H_2O_2$ without any pretreatment.

In the CSTR study, a 250-ml Pyrex filter flask equipped with a magnetic stirrer was used. This configuration allowed for optimal mixing and ensured that the reagents interacted effectively throughout the reaction process. To initiate the experiment, synthetic solution and Fenton-like reagents, each at the desired concentrations, were separately and continuously fed into the reactor using a multichannel peristaltic pump, which precisely regulated the flow rate of each component. By adjusting the flow rate accordingly, the required hydraulic retention time (HRT) was achieved. The temperature and pH of the solution in the reactor were controlled at 25 °C and 2.5, respectively, throughout the experiment. As the reactions progressed, the effluent was periodically collected from the overflow port of the reactor. This effluent was then subjected to analysis using the same methods established in the batch study. The sampling was conducted repeatedly until a steady-state condition was achieved, during which the concentrations of all reactants stabilized within the system.

## RESULTS AND DISCUSSION

### Determination of rate constant at standard-state condition

In an ideal batch reactor, the oxidation processes of the target pollutants, AP and AN, with OH• can be mathematically described by second-order reaction kinetics as mentioned previously. The respective rate expressions governing the decay of the concentrations of the pollutants over time are represented by Eqs. (7) and (8):

$$\frac{\mathrm{d[AP]}}{\mathrm{d}t} = -k_{\mathrm{AP,\,OH\bullet}}[\mathrm{OH\bullet}][\mathrm{AP}] \tag{7}$$

$$\frac{\mathrm{d[AN]}}{\mathrm{d}t} = -k_{\mathrm{AN,\,OH\bullet}}[\mathrm{OH\bullet}][\mathrm{AN}] \tag{8}$$

In this framework, the concept of competitive kinetics, where both pollutants exposed to the same concentration of OH• simultaneously, was applied. This leads to the derivation of Eq. (9), which illustrates the relationship between the decay of AP and AN in the ideal batch reactor. In this equation, $[\mathrm{AP}]_0$ and $[\mathrm{AN}]_0$ denote the initial molar concentrations of AP and AN, respectively, while $[\mathrm{AP}]_t$ and $[\mathrm{AN}]_t$ represent their concentrations at any given time. The slope derived from the linear relationship defined by Eq. (9) enables the determination of the ratio of the rate constants for the oxidation of AP and AN.

$$\ln\left(\frac{[\mathrm{AP}]_t}{[AP]_0}\right) = \frac{k_{\mathrm{AP,\,OH\bullet}}}{k_{\mathrm{AN,\,OH\bullet}}} \ln\left(\frac{[\mathrm{AN}]_t}{[AN]_0}\right) \tag{9}$$

To validate the experimental approach, several control experiments were conducted. Under the specific experimental conditions, neither AP nor AN was subject to volatilization. Furthermore, the potential for direct oxidation by $H_2O_2$ molecules, along with any adsorption onto ferric hydroxide ($Fe(OH)_3$) precipitates that formed after alkaline pretreatment prior to organic analysis, was found to be negligible.

To assess the accuracy and precision of the experimental setup as well as the laboratory analyses, triplicate experiments under identical initial conditions were performed (Runs #1 to #3 as shown in Table 1). The consistency of results across these runs is illustrated in Fig. 1. Notably, within the first 45 min of the reaction, a remarkable average removal efficiency of 97% for AP and 85% for AN were observed as depicted in Fig. 1a. However, once the $H_2O_2$ was totally exhausted at the 45th min, the degradation of both AP and AN ceased. This indicates that the complete consumption of $H_2O_2$ is a critical factor in the continuous oxidation process of the target pollutants. Additionally, Fig. 1a reveals a crucial insight regarding the reactivity of AP compared to AN; specifically, AP exhibited higher reactivity with OH•. This suggests that the $k_{\mathrm{AP,\,OH\bullet}}$ is likely greater than the $k_{\mathrm{AN,\,OH\bullet}}$.

The relationship between the natural logarithm of the molar concentration ratios of AP and AN was investigated, as evidenced by the linear plots corresponding to Eq. (9). The linearity of these plots was validated with coefficients of determination ($R^2$) exceeding 0.998 across all replicate experiments, as depicted in Fig. 1b. Each slope of these linear relationships, indicative of the ratio between the rate constants $k_{\mathrm{AP,\,OH\bullet}}$ and $k_{\mathrm{AN,\,OH\bullet}}$, yielded values of 1.9271, 1.9379, and 1.9212. These correspond to $k_{\mathrm{AP,\,OH\bullet}}$ values of$9.25\times10^9$, $9.30\times10^9$, and $9.22\times10^9$ 1/(M·s), respectively. The consistency of these results confirms the reliability and accuracy of the experimental setup as well as the laboratory analyses applied.

When comparing the oxidation rates of AP and AN in the Fenton-like process with those in the traditional Fenton process, a noteworthy distinction emerged, i.e., the rates in the Fenton-like process were significantly slower, as expected (Fig. 2a). Under identical conditions involving a fixed amount of iron (either in $Fe^{2+}$ or $Fe^{3+}$ form), the remaining concentrations of AP and AN after 60 min were 80.80% and 89.70%

**Table 1** Values of $k_{AP,\cdot OH}$ under batch studies with 60 min of reaction time.

| Run No. | $[AP]_0$ (mM) | $[AN]_0$ (mM) | $[Fe^{3+}]_0$ (mM) | $[H_2O_2]_0$ (mM) | $k_{AP,\cdot OH}$ (1/(M·s)) |
|---|---|---|---|---|---|
| 1 | 5 | 5 | 5 | 20 | $9.25\times10^9$ |
| 2 | 5 | 5 | 5 | 20 | $9.30\times10^9$ |
| 3 | 5 | 5 | 5 | 20 | $9.22\times10^9$ |
| 4 | 5 | 5 | 1 | 20 | $9.64\times10^9$ |
| 5 | 5 | 5 | 1 ($[Fe^{2+}]_0$) | 20 | $8.82\times10^9$ |
| 6 | 5 | 5 | 4 | 20 | $9.30\times10^9$ |
| 7 | 5 | 5 | 3 | 20 | $9.62\times10^9$ |
| 8 | 5 | 5 | 5 | 60 | $8.41\times10^9$ |
| 9 | 5 | 5 | 4 | 60 | $8.53\times10^9$ |
| 10 | 5 | 5 | 3 | 60 | $8.46\times10^9$ |
| 11 | 5 | 5 | 5 | 40 | $8.59\times10^9$ |
| 12 | 5 | 4 | 5 | 20 | $9.46\times10^9$ |
| 13 | 5 | 3 | 5 | 20 | $9.55\times10^9$ |

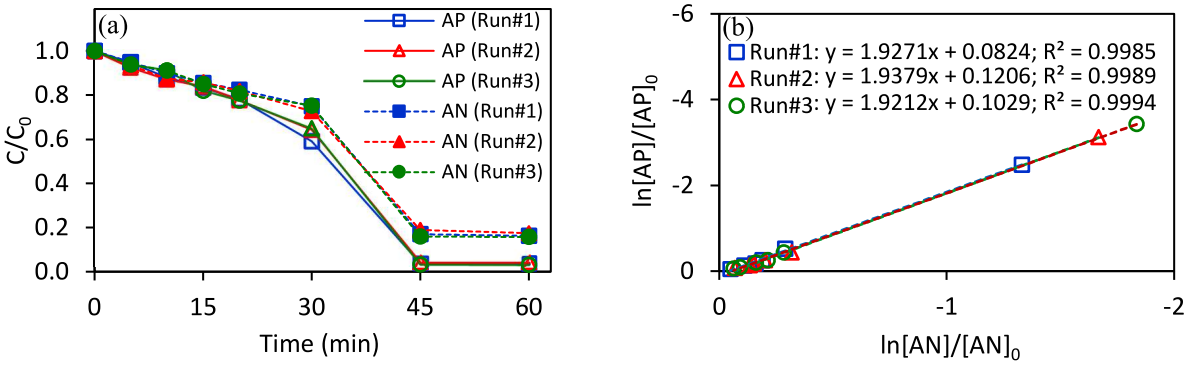


**Fig. 1** Triplicated experiments under the conditions of 5 mM AP, 5 mM AN, 5 mM $Fe^{3+}$, 20 mM $H_2O_2$, pH 2.5, and 25 °C: (a) organic degradation; (b) rate constant determination.

for the Fenton-like process, respectively, compared with 33.50% and 52.80% for the traditional Fenton process. Despite these differences in pollutant removal efficiencies, the calculated $k_{AP,\cdot OH}$ values, determined using the same methodology as previously mentioned, were comparable across both methods of $9.64 \times 10^9$ and $8.82 \times 10^9$ 1/(M·s), respectively, as illustrated in Fig. 2b and Table 1 (Runs #4 and #5).

The investigation into the various concentrations of reactants allows the evaluation of their influence on the reaction kinetics. The $Fe^{3+}$ concentration was systematically decreased from 5 mM to 4 mM and finally to 3 mM, while maintaining $H_2O_2$ at either 20 mM (Runs #1 to #3, #6, and #7) or 60 mM (Runs #8 to #10). Under both $H_2O_2$ concentrations, the disappearance rates of both AP and AN decelerated as

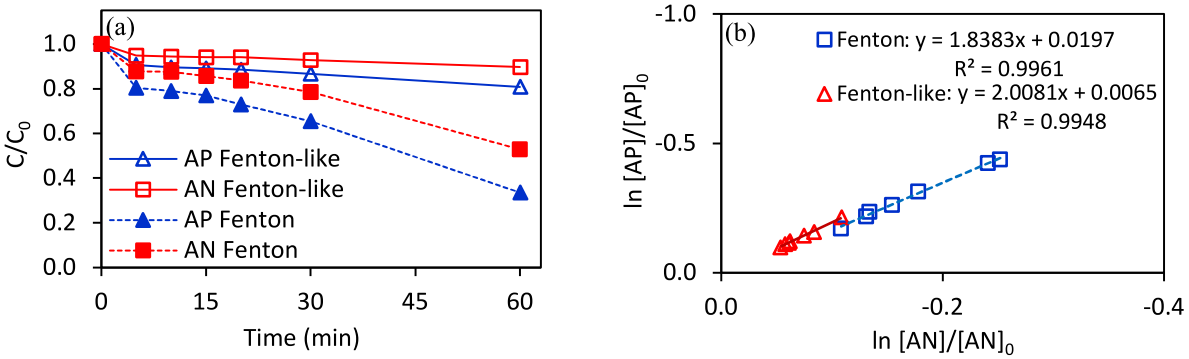


**Fig. 2** Comparison between Fenton and Fenton-like processes under the conditions of 5 mM AP, 5 mM AN, 20 mM $H_2O_2$, 1 mM $Fe_2^+$ (Fenton), or $Fe^{3+}$ (Fenton-like), pH 2.5, and 25 °C: (a) organic degradation; (b) rate constant determination.

$Fe^{3+}$ decreased, indicating $Fe^{3+}$ limitation under the studied conditions (data not shown). Nevertheless, subsequent analysis confirmed that the $k_{AP,\,OH\bullet}$ values remained consistent with those from prior conditions (Table 1), suggesting that variations in $Fe^{3+}$ concentration did not have any significant effect on $k_{AP,\,OH\bullet}$, which aligns with theoretical expectations.

To further assess the impact of $H_2O_2$, its concentration was sequentially changed from 20 mM (Runs #1 to #3) to 40 mM (Run #11) and finally to 60 mM (Run #8), while keeping $Fe^{3+}$ constant at 5 mM. Increasing the concentrations of $H_2O_2$ significantly accelerated the degradation of both AP and AN, i.e., complete degradation occurred at 20, 30, and 45 min, respectively, which was accompanied by an increase in $H_2O_2$ consumption. The observed scavenging effect from $H_2O_2$ was particularly evident, as concentrations were raised to 40 and 60 mM, demonstrating the reactive interactions among the constituents. Nevertheless, the $k_{AP,\,OH\bullet}$ values during these varying conditions remained stable, ranging from $8.41 \times 10^9$ to $8.59 \times 10^9$ 1/(M·s) (Table 1).

To assess the influence of organic concentration on the performance of the Fenton-like reaction, the concentration of AN was systematically reduced from 5 mM (Runs #1 to #3) to 4 mM (Run #12) and subsequently to 3 mM (Run #13). Throughout this investigation, the concentrations of AP, $Fe^{3+}$, and $H_2O_2$ were maintained constant at 5 mM each. The oxidation rates of AP exhibited no significant differences across the varying concentrations of AN, i.e., AP reduction profiles were comparable, and AP was completely oxidized at 45 min. This observation can largely be attributed to the $k_{AP,\,OH\bullet}$ values being nearly twice as high as those of $k_{AN,\,OH\bullet}$, suggesting that AP is more selective and susceptible to reaction with OH• compared to AN. As a result, AP retained its competitive advantage even within the studied concentration ranges. Moreover, the $k_{AP,\,OH\bullet}$ values derived from different AN concentration scenarios were comparable, as shown in Table 1.

In addition to the batch reactor experiments, a CSTR, with different forms of the mass balance equation, was also employed to validate the $k_{AP,\,OH\bullet}$ values obtained from the batch studies. By applying the competitive kinetics concept to an ideal CSTR operating at steady state, new equations to determine $k_{AP,\,OH\bullet}$ were formulated. Specifically, the mass balance equations for AP and AN in the CSTR at the steady state condition are expressed in Eqs. (10) and (11). In these equations, $V$ represents the effective volume of the reactor, while $Q_{inf}$ and $Q_{eff}$ signify the influent and effluent flow rates. Additionally, $[AP]_{inf}$ and $[AN]_{eff}$ denote the influent and effluent molar concentrations of AP and AN at steady state, respectively. Sequentially, Eq. (12) can be derived for the determination of the $k_{AP,\,OH\bullet}$ values using the parameter relationships defined above, thus facilitating a validation of the findings from the batch experiments.

$$V\frac{d[AP]}{dt} = 0 = Q_{inf}[AP]_{inf} - Q_{eff}[AP]_{eff} - k_{AP,\,OH\bullet}[AP]_{eff}[OH\bullet]_{eff}(V) \quad (10)$$

$$V\frac{d[AN]}{dt} = 0 = Q_{inf}[AN]_{inf} - Q_{eff}[AN]_{eff} - k_{AP,\,OH\bullet}[AN]_{eff}[OH\bullet]_{eff}(V) \quad (11)$$

$$\frac{k_{AP,\,OH\bullet}}{k_{AN,\,OH\bullet}} = \left(\frac{[AP]_{inf} - [AP]_{eff}}{[AN]_{inf} - [AN]_{eff}}\right)\left(\frac{[AN]_{eff}}{[AP]_{eff}}\right) \quad (12)$$

The impacts of $Fe^{3+}$, $H_2O_2$, and hydraulic retention time (HRT) on the $k_{AP,\,OH\bullet}$ were comprehensively examined. The results of these investigations are summarized in Table 2. The steady-state results from the CSTR experiments showed strong agreement with the batch study findings. AP demonstrated greater susceptibility to OH•attack compared to AN. The removal efficiencies for both compounds were significantly dependent on the concentrations of $Fe^{3+}$ and $H_2O_2$. In experiments with initial concentrations of 1 mM for both AP and AN, a $Fe^{2+}$ concentration of 0.5 mM (Run #14) proved inadequate for effective $H_2O_2$ decomposition catalysis with the removal efficiencies of 34.77% (AP) and 22.63% (AN). Increasing $Fe^{2+}$ to 1 mM (Run #15) resulted in substantial improvement in removal efficiencies for both compounds (41.15% (AP) and 28.11% (AN)), while further elevation to 1.5 mM (Run #16) provided lesser additional benefits (45.59% (AP) and 32.49% (AN)). Parallel behavior was observed with $H_2O_2$, where 20 mM concentration (Run #18) delivered optimal removal efficiency at a 15-min hydraulic retention time (46.38% (AP) and 31.48% (AN)). Progressive HRT extension from 15 to 30 and finally 60 min (Runs #15, #19, and #20) led to corresponding enhancements in AP and AN removal efficiency (41.15% to 52.74% and 60.90% (AP) and 28.11% to 38.03% and 46.69% (AN)). While $H_2O_2$ consumption exhibited direct correlation with both $Fe^{3+}$ concentration and HRT, measurable residual $H_2O_2$ persisted in all effluent samples (Table 2), thereby maintaining Fenton cycle continuity. However, given that both $Fe^{3+}$ and $H_2O_2$ can function as OH• scavengers, careful optimization of Fenton reagent ratios relative to pollutant concentrations is crucial for treatment efficacy. The $k_{AP,\,OH\bullet}$ values derived from the CSTR experiments following Eq. (12) showed a range from $8.36 \times 10^9$ to $9.17 \times 10^9$ 1/(M·s) as summarized in Table 2, which are considerably comparable to those observed in the batch mode experiments.

The average $k_{AP,\,OH\bullet}$ value calculated across all experimental scenarios was found to be $8.97 \times 10^9$ 1/(M·s). Notably, this average is in close agreement

**Table 2** Values of $k_{AP,OH\bullet}$ and steady-state (SS) concentrations under continuous studies.

| Run No. | $[Fe^{3+}]_{inf}$ (mM) | $[H_2O_2]$ (mM) | | [AP] (mM) | | [AN] (mM) | | HRT | $k_{AP,OH\bullet}$ |
|---|---|---|---|---|---|---|---|---|---|
| | | Influent | @ SS | Influent | @ SS | Influent | @ SS | (min) | (1/(M·s)) |
| 14 | 0.5 | 10.0 | 8.8 | 1.06 | 0.69 | 1.00 | 0.77 | 15 | $8.75\times10^9$ |
| 15 | 1 | 10.0 | 8.3 | 1.02 | 0.60 | 1.00 | 0.72 | 15 | $8.59\times10^9$ |
| 16 | 1.5 | 10.0 | 7.7 | 1.06 | 0.58 | 1.01 | 0.68 | 15 | $8.36\times10^9$ |
| 17 | 1 | 5.0 | 2.4 | 1.02 | 0.60 | 1.00 | 0.74 | 15 | $9.17\times10^9$ |
| 18 | 1 | 20.0 | 17.8 | 1.04 | 0.56 | 1.01 | 0.69 | 15 | $9.06\times10^9$ |
| 19 | 1 | 10.0 | 7.1 | 1.04 | 0.49 | 1.01 | 0.63 | 30 | $8.73\times10^9$ |
| 20 | 1 | 10.0 | 6.5 | 1.02 | 0.40 | 1.02 | 0.54 | 60 | $8.53\times10^9$ |

with the $9.29\times10^9$ 1/(M·s) reported for the traditional Fenton process ($Fe^{2+}/H_2O_2$) at pH 3.0 by Boonrattanakij et al [9], further validating the consistency and accuracy of these results. Additionally, the steady-state mass balance equations for AP and AN, as presented in Eqs. (10) and (11), can be utilized to estimate the molar concentration of OH• in the reactor at steady state ($[OH\bullet]_{ss}$). Since the mass balance accounts for known parameters, the $[OH\bullet]_{ss}$, which equals $[OH\bullet]_{eff}$, can be determined. The calculated values for $[OH\bullet]_{ss}$ ranged from $5.0\times10^{-14}$ to $1.1\times10^{-13}$ M, consistent with the values reported by Pignatello et al [22], highlighting the highly reactive and transient nature of OH• in the system.

**Effect of temperature**

This section aims to explore the thermal effects on the $k_{AP,OH\bullet}$, a topic that has not been previously examined, by using a batch reactor approach. The temperature dependence of reaction rate constants is often characterized by the Arrhenius equation, represented in Eq. (13). In this equation, $A_0$ is the frequency factor, $E_a$ is the activation energy, $R$ denotes the universal gas constant ($8.314\times10^{-3}$ kJ/(mol·K), and $T$ is the absolute temperature expressed in Kelvin. The Arrhenius constants, $A_0$ and $E_a$, can be derived from the linearized form of Eq. (13) as shown in Eq. (14):

$$k = A_0 \exp\left(-\frac{E_a}{RT}\right) \tag{13}$$

$$\ln k = \ln A_0 - \frac{E_a}{R}\left(\frac{1}{T}\right) \tag{14}$$

While this methodology offers a theoretical basis for assessing the temperature dependence, quantitatively determining these Arrhenius parameters in the context of the Fenton-like process presents distinct challenges. This complexity arises from the presence of multiple sequential reactions leading to the formation of OH•, as well as the competitive transformations involving all reactive substances. Current literature presents very limited temperature-dependent rate constants for these related reactions [23].

To address these intricacies, this research employs the quasi-steady-state approximation for OH• alongside the initial rate technique. Previous temperature-dependent kinetics studies often assume the OH• generation rate to be thermally independent, e.g., Chin and Wine [24] in a $H_2O_2$/UV system and Kowaguchi et al [25] in an $O_3/H_2O_2$ system. This assumption also aligns with the low activation energy for OH• formation reported by Buxton et al [7] and further supported by recent studies [26, 27], which highlight the minimal thermal influence on radical initiation in aqueous advanced oxidation processes. However, sequential reactions in homogeneous Fenton-like system are highly complex, as elaborated in previous works [22, 28], where multiple initiation, propagation, and termination steps govern OH• dynamics. To verify the validity of the existence of the quasi-steady state under Fenton-like conditions, the initial rate technique was adopted to minimize interference from competitive reactions between OH• and intermediates formed during AP oxidation. It is necessary to note that AN cannot serve as a reference compound in this part, as its temperature-dependent $k_{AP,OH\bullet}$ value is not available. Eq. (7) can be simplified to a pseudo 1st-order rate expression (Eq. (15)), a form widely used by several studies, including that of Chaisrisongkram et al [29]. In this equation, $k'_{AP,OH\bullet}$ represents the pseudo-first-order rate constant.

$$\left(\frac{d[AP]}{dt}\right)_0 = -k'_{AP,OH\bullet}[AP]_0 \tag{15}$$

A series of additional batch experiments were conducted with varying concentrations of AP ranging from 1 to 10 mM (without AN) while maintaining identical experimental conditions. Fig. 3a illustrates the concentration profiles of AP during the initial 2 min of the reaction and demonstrates that these profiles could be satisfactorily fitted using third-degree polynomial equations. This numerical approach has been successfully employed for slope estimation of non-linear curves in several studies [30–32]. The initial reaction rates, $(d[AP]/dt)_0$, were derived by differentiating these polynomial equations with respect to time and evaluating the limit as time approaches zero. The resulting plot of $(d[AP]/dt)_0$ against the initial concentration of AP, $[AP]_0$, indicated a linear

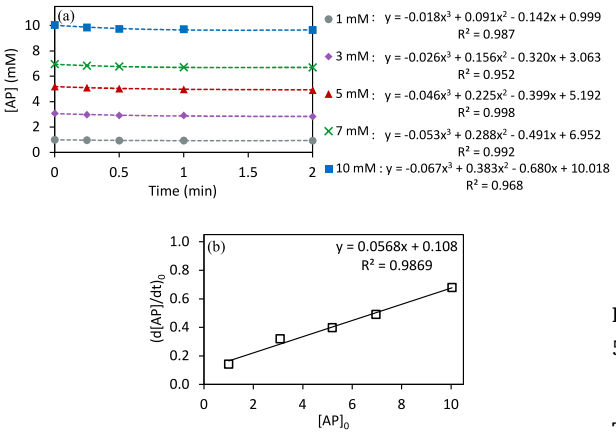


**Fig. 3** AP degradation by Fenton-like reaction under the conditions of 3 mM $Fe^{3+}$, 20 mM $H_2O_2$, pH 2.5, and 25 °C: (a) AP degradation; (b) relationship between the initial rate and the initial AP concentration.

relationship, exhibiting the $R^2$ of 0.9869, as shown in Fig. 3b.

This relationship implies that the initial disappearance rate of AP was solely dependent on the concentration of AP, suggesting that the OH• concentration generated during this initial phase remained relatively constant irrespective of the varying AP concentrations. This finding strongly supports the existence of a quasi-steady-state condition during the initial reaction phase under the experimental conditions, consistent with previous findings [24, 25]. This transient steady-state behavior has also been observed in other Fenton systems [33]. However, further analysis revealed that this proportionality only held during the initial stage, as subsequent rates, $(-\mathrm{d[AP]}/\mathrm{d}t)_t$, deviated from linearity with AP concentration, $[\mathrm{AP}]_t$, likely due to accumulating scavenging effects arising from intermediates [34, 35]. Thus, the quasi-steady-state approximation for [OH•] is only applicable during the brief initial phase under the experimental conditions. From the slope value derived from the linear plot (0.0568 1/min or $9.46 \times 10^{-4}$ 1/s) and the determined $k_{\mathrm{AP,\,OH\bullet}}$ value of $8.97\times10^9$ 1/(M·s), the quasi-steady-state concentration of OH• was calculated to be approximately $1.1 \times 10^{-13}$ M. This concentration range is notably low and aligns well with values observed in the CSTR studies and in Pignatello et al [22].

Furthermore, to explore the thermal effects on the degradation process, another set of batch experiments was performed under similar conditions, with temperature variations of 20, 25, 30, 35, and 40 °C (293, 298, 303, 308, and 313 K, respectively) including a duplicate run at 40 °C. The results clearly indicated that the oxidation rates of AP increased with rising temperatures and were appropriately fitted using third-degree polynomial equations similar to the case of

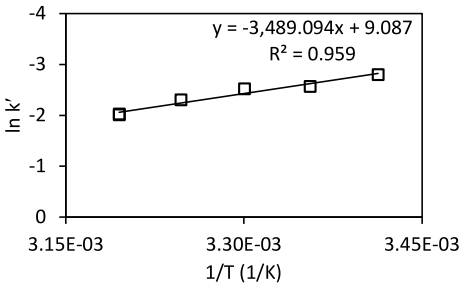


**Fig. 4** Effect of temperature on $k'_{\mathrm{AP,\,OH\bullet}}$ under conditions of 5 mM AP, 3 mM $Fe^{3+}$, 20 mM $H_2O_2$, and pH 2.5.

**Table 3** Activation energy ($E_a$) of the reactions between hydroxyl radicals and aromatic hydrocarbons in water.

| Compound | $E_a$ (kJ/mol) | Temperature (K) | Reference |
|---|---|---|---|
| Anthracene | 51.3 | 278–333 | [36] |
| Benzoate | 8.8 ± 0.6 | 284–343 | [37] |
| Benzene | 50.3 ± 2.5 | 288–305 | [38] |
| Phenol | 63.3 ± 2.3 | 288–305 | [38] |
| Toluene | 10.33 | 303–340 | [39] |
| Acetophenone | 29 | 293–313 | This study |

quasi-steady-state verification. The resulting $k'_{\mathrm{AP,\,OH\bullet}}$ at different temperatures were correlated using the linearized form of the Arrhenius equation (Eq. (14)), and the resulting fit is presented in Fig. 4. This analysis yielded the Arrhenius constants for $k'_{\mathrm{AP,\,OH\bullet}}$ of $8.84\times10^3$ 1/min or $1.47 \times 10^2$ 1/s and 29 kJ/mol for $A_0$ and $E_a$, respectively. This $E_a$ value should be identical for $k_{\mathrm{AP,\,OH\bullet}}$ as well, since the conversion from an intrinsic second-order to a pseudo-first-order preserves the exponential term in the Arrhenius equation (unlike the $A_0$, which incorporates [OH•]). Table 3 compares the $E_a$ value for AP oxidation by OH• obtained in this work with literature values for other aromatic hydrocarbons. Notably, the measured $E_a$ for AP falls at the middle of this reported range.

The Arrhenius equation for $k'_{\mathrm{AP,\,OH\bullet}}$ over the temperature range of 20 to 40 °C can be expressed as in Eq. (16). A comparison of the observed versus pre-

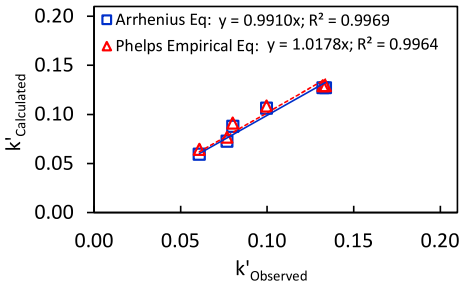


**Fig. 5** Plot between observed $k'_{\mathrm{AP,\,OH\bullet}}$ and calculated $k'_{\mathrm{AP,\,OH\bullet}}$.

dicted $k'_{AP,\,OH\bullet}$ values according to this Arrhenius equation produced a linear line with the slope of 0.9910 and the $R^2$ of 0.9969 as shown in Fig. 5, indicating the accuracy and reliability of the Arrhenius estimation.

$$k'(1/s) = 1.47 \times 10^2 \exp\left(-\frac{3{,}489.1}{T}\right) \quad (16)$$

Assuming that the OH• concentrations under quasi-steady-state conditions do not differ significantly between the 20 °C and 40 °C conditions, as demonstrated in previous studies [23, 24], the temperature-dependent $k_{AP,\,OH\bullet}$ can be approximated using the following expression (Eq. (17)). This provides valuable insight into the thermal response of the reaction kinetics, enhancing the applicability of the Fenton-like process regarding temperature variations in practical scenarios.

$$k_{AP,\,OH\bullet@T_2} \approx k_{AP,\,OH\bullet@T_1} \exp\left(-3{,}489.1\left(\tfrac{1}{T_2}-\tfrac{1}{T_1}\right)\right) \quad (17)$$

In addition to utilizing the Arrhenius equation to assess the temperature dependence of the $k'_{AP,\,OH\bullet}$ under quasi-steady-state conditions, the temperature-dependent $k'_{AP,\,OH\bullet}$ can also be characterized using a temperature correlation coefficient ($\theta$) in accordance with the Phelps empirical equation, as represented in Eq. (18). This empirical approach provides an alternative means of evaluating the effects of temperature on reaction kinetics.

$$k'_{AP,\,OH\bullet@T_2} = k'_{AP,\,OH\bullet@T_1}\,\theta^{T_2-T_1} \quad (18)$$

To determine the temperature correlation coefficient, a nonlinear least-squares method was applied, resulting in a calculated $\theta$ value of 1.035. Similar to the analysis conducted using the Arrhenius equation, the Phelps-calculated values of $k'_{AP,\,OH\bullet}$ demonstrated a strong correlation with the observed $k'_{AP,\,OH\bullet}$ values. The linear regression analysis yielded a slope of 1.0178 and the $R^2$ of 0.9964 (Fig. 5). This high degree of correlation further supports the reliability of applying the Phelps correlation for modeling the temperature dependence in the context of the Fenton-like oxidation process. Moreover, the determined $\theta$ value can be effectively applied to the rate constant $k_{AP,\,OH\bullet}$ under the assumption that the quasi-steady-state concentration of OH• remains independent of temperature, as shown in Eq. (19).

$$k_{AP,\,OH\bullet@T_1} \approx k_{AP,\,OH\bullet@T_2}(1.035)^{T_1-T_2} \quad (19)$$

The Arrhenius and Phelps equations developed in this research quantify the thermal effects on OH•-mediated reactions. Based on the reaction mechanisms proposed by Boonrattanakij et al [9], the degradation of AP by OH• under various temperatures can be simulated and precisely monitored. This provides vital information for designing and optimizing operational conditions for both Fenton-like and other AOPs.

## CONCLUSION

The $k_{AP,\,OH\bullet}$ was successfully determined through a combination of the Fenton-like process and a competitive kinetics approach. The values obtained for $k_{AP,\,OH\bullet}$ varied with different reactant concentrations, HRT, and operational modes, ranging from $8.36 \times 10^9$ to $9.64 \times 10^9$ 1/(M·s). The average $k_{AP,\,OH\bullet}$ across all experiments was calculated to be $8.97 \times 10^9$ 1/(M·s) at 25 °C and 1 atm. Notably, OH• could achieve a quasi-steady state during the initial period of the reaction under the studied conditions. Utilizing this quasi-steady-state approximation, the $E_a$ of the Arrhenius equation within the temperature range of 20 to 40 °C was 29 kJ/mol. Furthermore, the $\theta$ derived from the Phelps empirical equation was found to be 1.035. These temperature-correction coefficients enhance the application of the obtained $k_{AP,\,OH\bullet}$ values in varying ambient conditions, facilitating a broader application across different thermal environments. Additionally, calculated concentrations of OH• at quasi-steady-state conditions in the batch reactor and at steady state in the CSTR showed comparable results, ranging from $5.0 \times 10^{-14}$ to $1.1 \times 10^{-13}$ M.

*Acknowledgements*: This research was supported by the Petchra Pra Jom Klao Master's Degree Research Scholarship from King Mongkut's University of Technology Thonburi.

## REFERENCES

1. Godjevargova T, Ivanova D, Alexieva Z, Dimova N (2003) Biodegradation of toxic organic components from industrial phenol production waste waters by free and immobilized *Trichosporon cutaneum* R57. *Process Biochem* **38**, 915–920.
2. Chen D, Huo S, Cheng P, Cheng Y, Zhou N, Chen P, Ruan R (2021) Treatment and nutrient recovery from acetophenone based wastewater by an integrated catalytic intense pulsed light and *Tribonema* sp. cultivation. *Chem Eng Process Process Intensif* **160**, 108276.
3. Garrido-Cardenas JA, Esteban-Garcia B, Aguera A, Sanchez-Perez JA, Manzano-Agugliaro F (2020) Wastewater treatment by advanced oxidation process and their worldwide research trends. *Int J Environ Res Public Health* **17**, 17010170.
4. Jiang L, Zeng J, Zhang D, Chen F, Guo Y, Zeng Q, Zhang J (2025) Synthesis of $Fe_{0.82}O$/activated carbon as a degradation membrane with efficient Fenton catalytic performance. *ScienceAsia* **51**, ID 2025071.
5. Rayaroth MP, Aravindakumar CT, Shah NS, Boczkaj G (2022) Advanced oxidation processes (AOPs) based wastewater treatment – unexpected nitration side reactions – a serious environmental issue: A review. *Chem Eng J* **430**, 133002.
6. Theerakarunwong CD, Kaewthet O, Phanichphant S (2023) Potential effectiveness of visible-light-driven $Fe/TiO_2$ photocatalysts for degradation of dyes contaminated wastewater and their antibacterial activity. *ScienceAsia* **49**, 454–461.
7. Buxton GV, Greenstock CL, Helman WP, Ross AB (1988) Critical review of rate constants for reactions of hy-

drated electrons, hydrogen atoms and hydroxyl radicals ($^{\bullet}OH/^{\bullet}O^{-}$) in aqueous solution. *J Phys Chem Ref Data* **17**, 513–886.
8. Zhao MJ, Jung L (1995) Kinetics of the competitive degradation of deoxyribose and other molecules by hydroxyl radicals produced by the Fenton reaction in the presence of ascorbic acid. *Free Radic Res* **23**, 229–243.
9. Boonrattanakij N, Joysampao A, Pobsuktanasub T, Anotai J, Ruangchainikom C (2017) Treatability of phenol-production wastewater: Rate constant and pathway of dimethyl enyl carbinol oxidation by hydroxyl radicals. *J Environ Manage* **204**, 613–621.
10. Hu ZY, Xiang FY, Mao JQ, Ding YL, Tong SP (2022) Oxidative efficiency of ozonation coupled with electrolysis for treatment of acid wastewater. *Electrochem* **28**, 2104191.
11. Lu X (2024) An example of a wastewater treatment project for high concentrations of benzene, xylene, acetophenone, and DOPO generated in the production of phosphorus flame retardant. *Water Pract Technol* **19**, 4210–4226.
12. Irfan S, Khan SB, Lam SS, Ong HC, Din MAU, Dong F, Chen D (2022) Removal of persistent acetophenone from industrial waste-water via bismuth ferrite nanostructures. *Chemosphere* **302**, 134750.
13. Thiel TA, Obata K, Abdi FF, van de Krol R, Schomacker R, Schwarze M (2022) Photocatalysis hydrogenation of acetophenone on a titanium dioxide cellulose film. *RSC Adv* **12**, 7055–7065.
14. Babuponnusami A, Muthukumar K (2014) A review on Fenton and improvements to the Fenton process for wastewater treatment. *J Environ Chem Eng* **2**, 557–572.
15. Wang N, Zheng T, Zhang G, Wang P (2016) A review on Fenton-like processes for organic wastewater treatment. *J Environ Chem Eng* **4**, 762–787.
16. Du Y, Zhou M, Lei L (2006) Role of the intermediates in the degradation of phenolic compounds by Fenton-like process. *J Hazard Mater* **136**, 859–865.
17. Gallard H (2000) Kinetic modelling of Fe(III)/$H_2O_2$ oxidation reactions in dilute aqueous solution using atrazine as a model organic compound. *Water Res* **34**, 3107–3116.
18. Zhen G, Lu X, Wang B, Zhao Y, Chai X, Niu D, Zhao T (2013) Enhanced dewatering characteristics of waste activated sludge with Fenton pretreatment: Effectiveness and statistical optimization. *Front Environ Sci Eng* **8**, 267–276.
19. Anotai J, Panchanawaporn N, Boonrattanakij N, Lu MC (2011) Verification of competitive kinetics technique and oxidation kinetics of 2,6-dimethylaniline and *o*-toluidine by Fenton process. *J Hazard Mater* **188**, 269–273.
20. APHA (2017) *Standard Methods for the Examination of Water and Wastewater*, 23rd edn, American Public Health Association, Washington, DC.
21. Brandhuber P, Korshin G (2009) *Methods for the Detection of Residual Concentration of Hydrogen Peroxide in Advanced Oxidation Processes*. Water Reuse Foundation, USA.
22. Pignatello JJ, Oliveros E, MacKay A (2006) Advanced oxidation processes for organic contaminant destruction based on the Fenton reaction and related chemistry. *Crit Rev Environ Sci Technol* **36**, 1–84.
23. Ramos MDN, Lima JPP, Aguiar A (2024) Determination of activation energy from decolorization reactions of synthetic dyes by Fenton processes using the Behnajady–Modirshahla–Ghanbary kinetic model. *Catalysts* **14**, 273.
24. Chin YP, Wine PH (1992) Temperature dependence of the kinetics of the OH + $H_2O_2$ reaction in aqueous solution. *J Phys Chem* **96**, 2202–2207.
25. Kowaguchi M, Hidaka H, Nishimura K (2022) Temperature-independent $OH^{\bullet}$ generation in $O_3/H_2O_2$ systems: Mechanistic insights and implications for water treatment. *Environ Sci Technol* **56**, 7891–7900.
26. Gligorovski S, Strekowski R, Barbati S, Vione D (2015) Environmental implications of hydroxyl radicals ($^{\bullet}OH$). *Chem Rev* **115**, 13051–13092.
27. Miklos DB, Remy C, Jekel M, Linden KG, Drewes JE, Hübner U (2018) Evaluation of advanced oxidation processes for water and wastewater treatment: A critical review. *Water Res* **139**, 118–131.
28. Neyens E, Baeyens J (2003) A review of classic Fenton's peroxidation as an advanced oxidation technique. *J Hazard Mater* **98**, 33–50.
29. Chaisrisongkram C, Thiwawong T, Onlaor K, Tunhoo B (2024) Preparation of calcium oxide/graphitic carbon nitrides (CaO/g-C3N4) composite for photocatalyst dye degradation. *ScienceAsia* **50**, ID 2024066.
30. Gurol MD, Singer PC (1982) Kinetics of ozone decomposition: A dynamic approach. *Environ Sci Technol* **16**, 377–383.
31. Leach RA, Carter CA, Harris JM (1984) Least-squares polynomial filters for initial point and slope estimation. *Anal Chem* **56**, 2304–2307.
32. Stojan J, Colicnik M, Fournier D (2004) Rational polynomial equation as an unbiased approach for the kinetic studies of *Drosophila melanogaster* acetylcholinesterase reaction mechanism. *BBA* **1703**, 53–61.
33. de Laat J, Le GT, Legube B (2004) A comparative study of the effects of chloride, sulfate, and nitrate ions on the rates of decomposition of $H_2O_2$ and organic compounds by $Fe^{2+}/H_2O_2$ and $Fe^{3+}/H_2O_2$. *Chemosphere* **55**, 715–723.
34. Brillas E, Sirés I, Oturan MA (2009) Electro-Fenton process and related electrochemical technologies based on Fenton's reaction chemistry. *Chem Rev* **109**, 6570–6631.
35. Oturan MA, Aaron JJ (2014) Advanced oxidation processes in water/wastewater treatment: Principles and applications. A review. *Crit Rev Environ Sci Technol* **44**, 2577–2641.
36. Diaz-Uribe C, Vallejo W, Quinones C (2020) Physical-chemical study of anthracene selective oxidation by a Fe(III)-phenylporphyrin derivative. *Int J Mol Sci* **21**, 353.
37. Poskrebyshev GA, Neta P, Huie RE (2002) Temperature dependence of the acid dissociation constant of the hydroxyl radical. *J Phys Chem A* **106**, 11488–11491.
38. Heath AA, Ehrenhauser FS, Valsaraj KT (2013) Effects of temperature, oxygen level, ionic strength, and pH on the reaction of benzene with hydroxyl radicals in aqueous atmospheric systems. *J Environ Chem Eng* **1**, 822–830.
39. Mao Y, Yang L, Liu S, Song Y, Luo M, Guo Y (2024) A theoretical study on toluene oxidization by OH radical. *BMC Chem* **18**, 72.